Lithium-Ion Batteries

Deutsche Ausgabe: DOI: 10.1002/ange.201601119
Internationale Ausgabe: DOI: 10.1002/anie.201601119

# A Sulfur Heterocyclic Quinone Cathode and a Multifunctional Binder for a High-Performance Rechargeable Lithium-Ion Battery

*Ting Ma[+], Qing Zhao[+], Jianbin Wang, Zeng Pan, and Jun Chen**

***Abstract:*** *We report a rational design of a sulfur heterocyclic quinone (dibenzo[b,i]thianthrene-5,7,12,14-tetraone = DTT) used as a cathode (uptake of four lithium ions to form $Li_4DTT$) and a conductive polymer [poly(3,4-ethylenedioxythiophene):poly(styrenesulfonate) = PEDOT:PSS) used as a binder for a high-performance rechargeable lithium-ion battery. Because of the reduced energy level of the lowest unoccupied molecular orbital (LUMO) caused by the introduced S atoms, the initial Li-ion intercalation potential of DTT is 2.89 V, which is 0.3 V higher than that of its carbon analog. Meanwhile, there is a noncovalent interaction between DTT and PEDOT:PSS, which remarkably suppressed the dissolution and enhanced the conductivity of DTT, thus leading to the great improvement of the electrochemical performance. The DTT cathode with the PEDOT:PSS binder displays a long-term cycling stability (292 $mAh\,g^{-1}$ for the first cycle, 266 $mAh\,g^{-1}$ after 200 cycles at 0.1 C) and a high rate capability (220 $mAh\,g^{-1}$ at 1 C). This design strategy based on a noncovalent interaction is very effective for the application of small organic molecules as the cathode of rechargeable lithium-ion batteries.*

Organic compounds have received great attention as active materials for electrodes of rechargeable batteries because of their structural diversity, renewability, low costs, and environment friendliness.[1] Organic carbonyl compounds especially quinones are one of the most promising candidates because of their high theoretical energy density and fast reaction kinetics.[2] However, most quinones have issues such as a relatively low reduction potential, high solubility in organic electrolytes, and poor electronic conductivity.[3] Introduction of sulfur heteroatoms can tune the lowest unoccupied molecular orbital (LUMO) energy of organic compounds and affect the reduction potential.[4] For example, anthraquinone shows a LUMO energy of −3.2 eV and a reduction potential at 2.27 V versus $Li^+/Li$. After introducing S to gain benzo[1,2-*b*:4,5-*b*′]dithiophene-4,8-dione (BDTD), the LUMO energy decreases to −3.5 eV, corresponding to an improved reduction potential at 2.52 V.[4d] Moreover, another carbonyl-based organic molecule, 5,7,12,14-pentacenetetrone (PT), with an extended π-conjugated configuration shows an initial reduction potential at 2.6 V.[5] After addition of S to PT the LUMO energy decreases and the obtained dibenzo-[*b*,*i*]thianthrene-5,7,12,14-tetraone (DTT) should show several advantages: 1) a multi-electron redox reaction provided by the quinoid structure should be possible; 2) an increased electronic conductivity[6] and DTT is less readily dissoluble[7] in an electrolyte than other nonconjugated organic molecules because of the extended π-conjugated configuration; 3) an enhanced reduction potential caused by the introduction of a S heteroatom.

The issues of low electronic conductivity and severe solubility for quinones are normally resolved by adding various conductive additives such as carbon materials.[8] However, the binder as another major component of the electrode, is rarely taken into consideration to settle these issues. Poly(vinylidene fluoride) (PVdF) as the most popular traditional binder is an electronic isolating polymer.[9] This insulating feature is counteracting the electronic conductivity of the electrode. Conductive polymers (like polyaniline, polypyrrole, polythiophene and their derivatives) have been widely used in various electrical applications because of their excellent chemical stability and high electrical conductivity.[10] Furthermore, some conductive polymers such as poly(3,4-ethylenedioxythiophene):poly(styrenesulfonate) (PEDOT:PSS) from the polythiophene family has been proposed as a binder for some inorganic electrodes.[11] Moreover, PEDOT with π-conjugated thiophene rings carries positive charges. The dissociated sulfonate groups in PSS balance the charges of the cationic PEDOT by forming a stable salt.[12] Therefore, PEDOT has the potential of being an electron acceptor, which would support its interaction with some organic electron donor molecules like DTT. Thus, PEDOT:PSS should be a good choice for a binder in organic electrodes.

Herein, we report a sulfur heterocyclic quinone (DTT, Scheme 1a) as cathode which combined with conductive

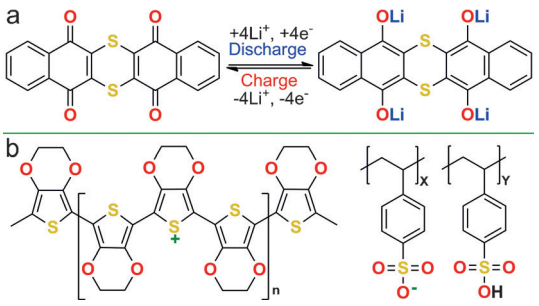


***Scheme 1.*** a) Structure and reversible electrochemical redox mechanism of DTT/$Li_4$DTT (DTT $M_w$ = 376 $g\,mol^{-1}$, theoretical specific capacity of 285 $mAh\,g^{-1}$). b) The polymeric structure of PEDOT:PSS.

[*] Dr. T. Ma,[+] Dr. Q. Zhao,[+] Dr. J. Wang, Dr. Z. Pan, Prof. J. Chen
Key Laboratory of Advanced Energy Materials Chemistry and State Key Laboratory of Elemento-Organic Chemistry
College of Chemistry, Nankai University, Tianjin 300071 (China)
E-mail: chenabc@nankai.edu.cn

[+] These authors contributed equally to this work.

Supporting information for this article can be found under: http://dx.doi.org/10.1002/anie.201601119.

polymer (PEDOT:PSS, Scheme 1 b) as multifunctional binder for rechargeable lithium-ion battery with high performance. The molecular design strategy allows the DTT molecule to achieve the three above-mentioned advantages. Furthermore, PEDOT:PSS plays multiple roles, which include binder function, conductive additive, and more importantly, an anchor base and coating to prevent DTT from dissolution. DTT and PEDOT:PSS can interact with each other because of the electron transfer of extended π-conjugated configuration of DTT (an electron donor) and cationic PEDOT (an electron acceptor), which results in noncovalent interaction between them. This interaction is beneficial to further suppress the dissolution of DTT into the electrolyte, which accordingly exhibits long-term cycling stability and high-rate capability in rechargeable lithium-ion battery.

DTT ($C_{20}H_8O_4S_2$, Scheme 1 a) was synthesized in two steps (Scheme S1, for details see the Supporting Information).[13] The obtained sample was characterized by Fourier transform infrared spectroscopy (FTIR), $^1$H-NMR spectroscopy, and high-resolution mass spectometry (HRMS; Figure S1). The product was in the form of dark purple powers with rob-like morphology on the micrometer scale (Figure S2). To study the electrochemical activity, DTT was combined with super-P and PVDF (6:3:1) to prepare the electrode and then assemble into coin 2032 cells versus lithium anode (detailed in the Supporting Information). 2 M lithium bis(trifluoromethanesulfonyl)imide (LiTFSI) in 1,3-dioxolane (DOL)/dimethoxyethane (DME) electrolyte with 1 wt% $LiNO_3$ additive was chosen as an optimized electrolyte[14] (detailed in the Supporting Information). For a comparison, the electrochemical performance of DTT with commercial ester-based electrolyte underwent fast capacity fading (Figure S3). There are three reduction peaks (at 2.85, 2.33, and 1.55 V) and four oxidation peaks (at 2.60, 2.87, 3.17, and 3.52 V) in the cyclic voltammogram (CV, Figure 1 a), which coincide with three discharge plateaus and four charge plateaus of the galvanostatic discharge/charge curves (Figure 1 b). The total areas of the oxidation and reduction peaks (Figure S4) are approximately equal, reassuring the high reversibility of the reactions.[2b] The discharge/charge capacity shows that DTT is used reversible in four Li-ion electrochemical reactions with the redox couples $Li_4C_{20}H_8O_4S_2$/$C_{20}H_8O_4S_2$ at the electrodes. There are four oxidation peaks/charge plateaus, but only three reduction peaks/discharge plateaus in the CV/galvanostatic curves. According to the capacity distribution, this phenomenon emerged because the reduction steps (LiDTT/$Li_2$DTT/$Li_3$DTT) occur very fast and the voltage gap between the two steps is too small to distinguish the steps. In addition, the voltage hysteresis results in a voltage gap between the redox peaks. Some conjugated carbonyl-based organic molecules and metal fluorides/oxides with multi-electron reactions also show the same phenomenon.[2b,15] To further verify the reversible electrochemical redox mechanism of DTT, the discharge/recharge products were examined by ex situ X-ray diffraction (XRD) and Raman spectroscopic measurements. Figure 1 c compares the XRD patterns of the initial DTT electrode at specific discharge/recharge states in a potential range of 1.6 to 3.6 V. During the discharge process, the XRD peaks ascribed to the initial structure of DTT become weak and disappear at the full discharge state (curve c in Figure 1 c). In the subsequent recharging process, the XRD patterns of the electrodes are reversed to the original forms (curve g in Figure 1 c). Such changes in the XRD patterns during the discharge/recharge process are generally observed for the electrodes of lithium- or sodium-ion batteries with crystalline organic active materials.[16] The Raman spectra were collected at the same states as the XRD test (Figure 1 d). The vibrations at 1648 $cm^{-1}$ and 1580 $cm^{-1}$ indicate the presence of a quinonoid carbonyl group (C=O).[13] These C=O peaks are gradually weakened during the discharge process (curve c in Figure 1 d), and recovered during the recharge process (curve g in Figure 1 d). Thus, the above observations reveal that the redox reactions of DTT during the lithiation/delithiation process is reversible and the C=O groups are active sites, which further supports the cyclic voltammetry (CV) and galvanostatic discharge/charge studies. More importantly, the initial discharge potential of DTT is 2.89 V, which is 0.3 V higher than for its carbon analog (PT; Figure S5). This result is in accordance with our expectation and further confirms the benefits of the S atom for the enhancement of the reduction potential.

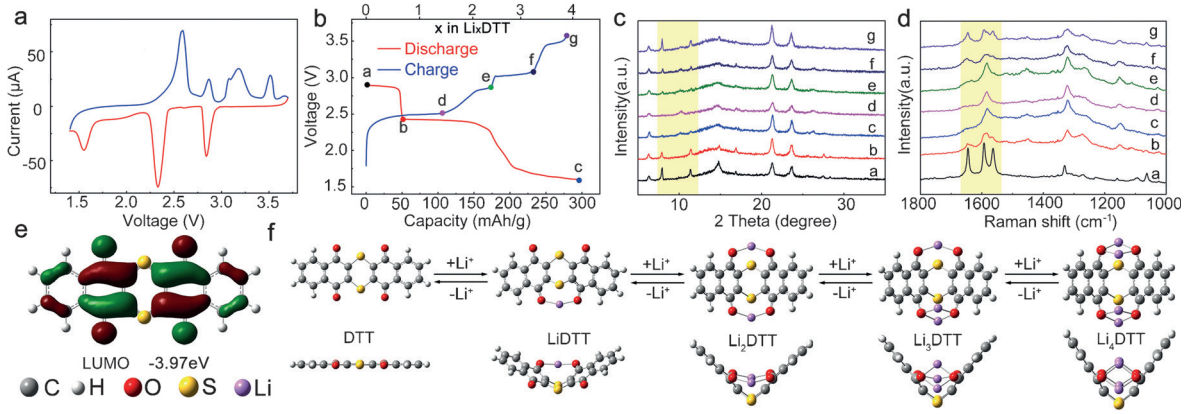


***Figure 1.*** a) CV curves of the cells with DTT cathode in the voltage range of 1.6–3.6 V at a scan rate of 0.1 $mV s^{-1}$. b) Corresponding galvanostatic discharge/charge curves with marked points at different discharge and recharge states (0.1 C rate, 1 C = 285 $mA g^{-1}$). c) XRD and d) Raman at the marked states in Figure 1 b. e) LUMO plot of DTT. f) The top and side views of optimized configurations of $Li_x$DTT ($x$ = 0–4) at different lithiation stages.

  

For better understanding the function of S atom, density functional theory (DFT) was performed to calculate the LUMO energy level of DTT (Figure 1e) and PT (Figure S6) (the computational details are given in the Supporting Information). The LUMO energy level of DTT and PT is −3.97 eV and −3.76 eV, respectively. In theory, the LUMO energy level correlates to the reduction potential, while a lower LUMO energy level corresponds to a higher reduction potential.[4a,c,17] As for carbonyl-based organic molecules, the S atom can reduce the LUMO energy level, which is accompanied by a raising reduction potential. Combined with the experimental and theoretical results, we can conclude that the reduction potential of DTT is enhanced significantly in comparison with PT by introducing the S atom. The configurations of the discharge products were also predicted by the DFT method (Cartesian coordination of the optimized structures are shown in Tables S1–S6). One DTT molecule can take up four Li-ions. The optimized structures for different lithiation stages ($Li_xDTT$) are shown in Figure 1f. Specifically, DTT is a planar molecule, but it bends while lithium atoms insert. The bending geometries of the lithiation products show that every lithium atom coordinates with two oxygen atoms to strengthen the binding with DTT. Furthermore, the binding energy ($E_b$, the definition of $E_b$ is shown in the Supporting Information) of $Li_4DTT$ is −12.76 eV, which indicates that DTT can firmly take up four lithium atoms to form the thermodynamically stable $Li_4DTT$. Thus, the DTT cathode with the four-electron redox reaction has increased discharge potentials because of the reduced LUMO energy by introduced by the S atom.

In order to improve the electrochemical performance of DTT electrode, we employed PEDOT:PSS as a binder with the consideration of excellent conductivity and electron acceptor character of PEDOT. The optimized electrode component ratio of DTT:super-P:PEDOT:PSS is 6:3:1 in this work (details are given in the Supporting Information, Figures S7–S10). To further explore the interaction between DTT and PEDOT:PSS, two materials, pristine DTT and a DTT-PEDOT:PSS composite (preparation details in the Supporting Information), were characterized by transmission electron microscopy (TEM). Pristine DTT exsisted in the form of bulk crystals with an in general orderly single-crystal lattice (Figure S11a–c). In contrast, DTT-PEDOT:PSS shows nanosized DTT particles (< 10 nm), which are encapsulated by a PEDOT:PSS coating (Figure 2a,b). The selected area electron diffraction image (SAED) of DTT-PEDOT:PSS (Figure 2c) reveals fuzzy rings patterns of PEDOT:PSS. Diffused rings and bright spots indicate the random crystallographic orientations of the DTT molecule and the polycrystalline electron diffraction pattern. The TEM images and the SAED pattern changes indicate that DTT can achieve the crystalline structural rearrangement by combining with PEDOT:PSS. This leads to a morphology change from micron bulk DTT crystals into well-coated DTT nanoparticles, and further infers that DTT can interact with the PEDOT:PSS binder effectively at molecular level.[18] This molecularly level interaction with coating effect can provide better isolation of DTT from the electrolyte and then inhibit the dissolution.

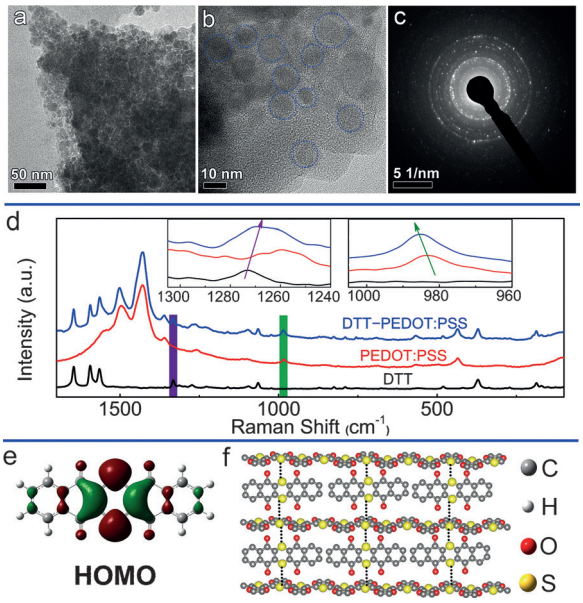


***Figure 2.*** Characterization of noncovalent interaction between DTT and PEDOT:PSS. a) TEM, b) HRTEM, and c) SAED of DTT-PEDOT:PSS composite. d) Raman spectra of DTT, PEDOT:PSS and their composite. e) The HOMO plot of DTT. f) The schematic diagram of interaction between DTT and PEDOT:PSS.

To further study the interactions between DTT and PEDOT:PSS at molecular level, Raman spectra, UV/Vis spectra, and the X-ray absorption near edge structure (XANES) were measured (details including the sample preparation can be found in the Supporting Information). The Raman spectra of DTT, PEDOT:PSS, and their composite are compared in Figure 2d. The stretching vibrations at 982 and 1272 $cm^{-1}$ represents the C–S bond of the thiophene ring in PEDOT[19] and the thianthrene ring in DTT,[13] respectively. As seen in the Raman data of DTT-PEDOT:PSS, the stretching vibration of the C–S bond generates a blue shift to 985 $cm^{-1}$ in PEDOT:PSS, while a red shift to 1267 $cm^{-1}$ is observed for DTT. These Raman shifts indicate that there is a noncovalent interaction between DTT and PEDOT:PSS,[18] which weakens the C–S bond of DTT and strengthens the C–S bond of PEDOT:PSS. More evidence for this noncovalent interaction between DTT and PEDOT:PSS can be found in the UV/Vis (Figure S12)[20] and X-ray absorption near-edge spectra (Figure S13; details can be found in the Supporting Information).[21]

To get further insight into the interaction sites between DTT and PEDOT:PSS, the highest occupied molecular orbital (HOMO) of DTT has been calculated by DFT. As shown in Figure 2e, the electron cloud is mainly located on the thianthrene ring of DTT, especially on the sulfur atoms. Therefore, the proposed probable interaction mechanism shows that the thiophene rings (positive charges) in PEDOT interact with the sulfur atoms in DTT through a noncovalent electrostatic interaction (PEDOT-$S^{\delta+}\cdots S^{\delta-}$-DTT, Figure 2f). Remarkably, benefiting from this interaction and the coating effect, the PEDOT:PSS prevents the dissolution of DTT into the electrolyte. Therefore, we infer that this PEDOT:PSS conductive binder can make contributions on the high-rate

capability as well as the cycling stability of batteries. The electrochemical behavior of the DTT cathode with PEDOT:PSS binder was investigated. CV proves that PEDOT:PSS shows good electrochemical stability in the potential range and has no influence on the electrochemical redox mechanism of DTT (Figure S14). Figure 3a shows the Nyquist plots of the electrodes with PVdF and PEDOT:PSS binders. The inset in Figure 3a is the equivalent circuit of the Nyquist plots. It indicates that the DTT electrode with

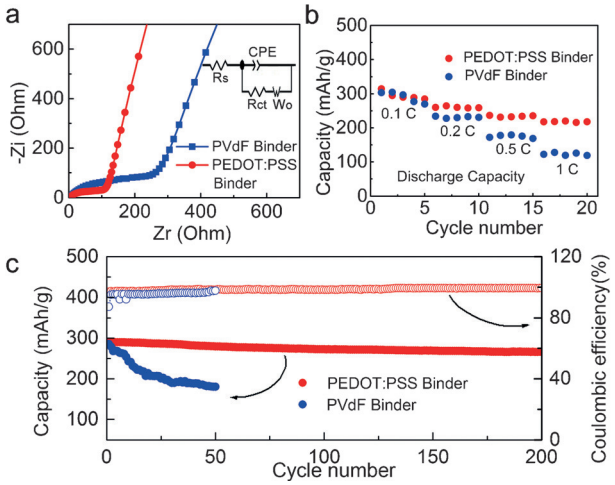


***Figure 3.*** Electrochemical properties of DTT cathode with PEDOT:PSS and PVdF binder. a) Electrochemical impedance spectroscopy, inset is corresponding equivalent circuit, $R_{ct}$ is the charge–transfer resistance and $W_0$ is the Warburg impendence. b) Rate capability and c) cycling stability with coulombic efficiency (0.1 C).

PEDOT:PSS binder exhibits a lower charge-transfer resistance than that with PVdF binder ($R_{ct}$(PEDOT:PSS) = 106.1 Ω, $R_{ct}$(PVdF) = 244.7 Ω). Furthermore, we compared the rate capability and cycling performance of the DTT cathode with PEDOT:PSS binder and PVdF binder. Figure 3b shows the rate capability of DTT electrode with PEDOT:PSS and PVdF binder at different current rates, respectively. The capacities of the DTT electrode with PEDOT:PSS binder obtained at 0.2, 0.5, and 1 C are 261, 231, and 220 mAh g$^{-1}$, respectively, all of which are higher than that of the PVdF binder electrode at the same rate. Moreover, the rate capability of the PEDOT:PSS binder electrode drops much less than that of the PVdF binder one at a high current rate (e.g., the rate capability of PVdF binder electrode at 1 C is 128 mAh g$^{-1}$, which is only 58 % of the rate capability of the PEDOT:PSS binder electrode). As displayed in Figure 3c, DTT electrode with PEDOT:PSS binder delivers 266 mAh g$^{-1}$ discharge capacity after 200 cycles at 0.1 C, which corresponds to capacity retention of 93 % compared to the theoretical specific capacity (285 mAh g$^{-1}$). The coulombic efficiency is close to 99 % during the whole cycling test. The capacity contribution from PEDOT:PSS was negligible in comparison with the high capacity of DTT (Figure S15). As comparison, the capacity is 181 mAh g$^{-1}$ with PVdF binder at 0.1 C after 50 cycles. These results indicate that DTT cathode with PEDOT:PSS binder exhibits much better electrochemical performance than the electrode with PVdF binder.

In order to verify the role of PEDOT:PSS binder on suppressing the dissolution of DTT, we disassembled the cycled cells to examine the conditions of the separators. The separator corresponding to PEDOT:PSS binder is almost no color change, while the one to PVdF binder becomes light green owing to the dissolution of DTT (Figure S16). This can further evidence that PEDOT:PSS binder is able to suppress the dissolution of DTT effectively. Therefore, we can conclude that the multifunctional PEDOT:PSS binder really benefits to enhance the rate capability and improve the cycling stability of battery due to its conductive feature and the interaction with DTT. To investigate the universality of the PEDOT:PSS binder, further studies of the analogous BDTD with either PEDOT:PSS or PVdF binder as cathode were conducted. The BDTD electrodes with PEDOT:PSS binder also exhibits better performance than that with PVdF binder (Figures S17–S19). Another strategy is to synthesize DTT-based functional polymer for reducing the dissolution and enhancing the performance. Thus, further efforts in this respect are still worth conducting.

In conclusion, we sucessfully design a DTT cathode with conductive polymer PEDOT:PSS as multipurpose binder for rechargeable lithium-ion battery. By introducing S atoms, DTT exhibits an initial high reduction potential at 2.89 V. DTT were reversibly cycled at potential window of 1.6–3.6 V with the redox couples of $Li_4C_{20}H_8O_4S_2/C_{20}H_8O_4S_2$. The electrochemical performance of DTT cathode has been signifcantly improved by employing PEDOT:PSS as multiple-role conductive binder, delivering a high discharge capacity of 292 mAh g$^{-1}$ in the 1st cycle at 0.1 C with uptake of four lithium ions to form $Li_4$DTT. Such an electrode shows 266 mAh g$^{-1}$ after 200 cycles at 0.1 C, which is still 93 % of the theoretical value. Furthermore, the DTT electrode provides high discharge capacities at high current rates (261 mAh g$^{-1}$ at 0.2 C, 231 mAh g$^{-1}$ at 0.5 C, and 220 mAh g$^{-1}$ at 1.0 C). Our results show that DTT with the PEDOT:PSS electrode is promising in the application of rechargeable lithium-ion batteries due to the rational LUMO and HOMO energy, and noncovalent interactions between DTT and PEDOT:PSS. As a promising binder candidate, PEDOT:PSS should obtain more applications in rechargeable batteries using organic electrodes.

## Acknowledgements

We thank the staff of National Synchrotron Radiation Laboratory in Hefei, China, in particular Prof. Li Song for the near edge absorption spectrum. This work was supported by National NSFC (grant number 21231005), MOE (grant numbers B12015 and IRT13R30) and Tianjin (grant number 13JCQNJC06400).

**Keywords:** lithium-ion batteries · molecular design · multifunctional binders · noncovalent interactions · sulfur heterocyclic quinones

  

**How to cite:** *Angew. Chem. Int. Ed.* **2016**, *55*, 6428 – 6432
*Angew. Chem.* **2016**, *128*, 6538 – 6542

[1] a) M. Armand, J. M. Tarascon, *Nature* **2008**, *451*, 652 – 657; b) Y. Zhao, Y. Ding, J. Song, G. Li, G. Dong, J. B. Goodenough, G. Yu, *Angew. Chem. Int. Ed.* **2014**, *53*, 11036 – 11040; *Angew. Chem.* **2014**, *126*, 11216 – 11220; c) J. C. Bachman, R. Kavian, D. J. Graham, D. Y. Kim, S. Noda, D. G. Nocera, S. H. Yang, S. W. Lee, *Nat. Commun.* **2015**, *6*, 7040; d) N. S. Choi, Z. Chen, S. A. Freunberger, X. Ji, Y. K. Sun, K. Amine, G. Yushin, L. F. Nazar, J. Cho, P. G. Bruce, *Angew. Chem. Int. Ed.* **2012**, *51*, 9994 – 10024; *Angew. Chem.* **2012**, *124*, 10134 – 10166; e) Y. Liang, Z. Tao, J. Chen, *Adv. Energy Mater.* **2012**, *2*, 742 – 769.

[2] a) B. Häupler, A. Wild, U. S. Schubert, *Adv. Energy Mater.* **2015**, *5*, 1402034; b) D. Chen, A. J. Avestro, Z. Chen, J. Sun, S. Wang, M. Xiao, Z. Erno, M. M. Algaradah, M. S. Nassar, K. Amine, Y. Meng, J. F. Stoddart, *Adv. Mater.* **2015**, *27*, 2907 – 2912; c) N. Ogihara, T. Yasuda, Y. Kishida, T. Ohsuna, K. Miyamoto, N. Ohba, *Angew. Chem. Int. Ed.* **2014**, *53*, 11467 – 11472; *Angew. Chem.* **2014**, *126*, 11651 – 11656; d) S. Wang, L. Wang, Z. Zhu, Z. Hu, Q. Zhao, J. Chen, *Angew. Chem. Int. Ed.* **2014**, *53*, 5892 – 5896; *Angew. Chem.* **2014**, *126*, 6002 – 6006.

[3] a) H. Wang, P. Hu, J. Yang, G. Gong, L. Guo, X. Chen, *Adv. Mater.* **2015**, *27*, 2348 – 2354; b) Z. Song, Y. Qian, M. L. Gordin, D. Tang, T. Xu, M. Otani, H. Zhan, H. Zhou, D. Wang, *Angew. Chem. Int. Ed.* **2015**, *54*, 13947 – 13951; *Angew. Chem.* **2015**, *127*, 14153 – 14157; c) W. Huang, Z. Zhu, L. Wang, S. Wang, H. Li, Z. Tao, J. Shi, L. Guan, J. Chen, *Angew. Chem. Int. Ed.* **2013**, *52*, 9162 – 9166; *Angew. Chem.* **2013**, *125*, 9332 – 9336; d) B. Genorio, K. Pirnat, R. Cerc-Korosec, R. Dominko, M. Gaberscek, *Angew. Chem. Int. Ed.* **2010**, *49*, 7222 – 7224; *Angew. Chem.* **2010**, *122*, 7380 – 7382; e) C. Luo, R. Huang, R. Kevorkyants, M. Pavanello, H. He, C. Wang, *Nano Lett.* **2014**, *14*, 1596 – 1602; f) Z. Zhu, M. Hong, D. Guo, J. Shi, Z. Tao, J. Chen, *J. Am. Chem. Soc.* **2014**, *136*, 16461 – 16464.

[4] a) G. S. Vadehra, R. P. Maloney, M. A. Garcia-Garibay, B. Dunn, *Chem. Mater.* **2014**, *26*, 7151 – 7157; b) Y. Liang, P. Zhang, J. Chen, *Chem. Sci.* **2013**, *4*, 1330 – 1337; c) K. Hernández-Burgos, S. E. Burkhardt, G. G. Rodríguez-Calero, R. G. Hennig, H. D. Abruña, *J. Phys. Chem. C* **2014**, *118*, 6046 – 6051; d) Y. Liang, P. Zhang, S. Yang, Z. Tao, J. Chen, *Adv. Energy Mater.* **2013**, *3*, 600 – 605; e) S. Debnath, A. Bedi, S. S. Zade, *Polym. Chem.* **2015**, *6*, 7658 – 7665; f) C. Wang, H. Dong, W. Hu, Y. Liu, D. Zhu, *Chem. Rev.* **2012**, *112*, 2208 – 2267.

[5] M. Yao, H. Senoh, T. Sakai, T. Kiyobayashi, *Int. J. Electrochem. Sci.* **2011**, *6*, 2905 – 2911.

[6] a) J. Wu, X. Rui, G. Long, W. Chen, Q. Yan, Q. Zhang, *Angew. Chem. Int. Ed.* **2015**, *54*, 7354 – 7358; *Angew. Chem.* **2015**, *127*, 7462 – 7466; b) C. Wang, Y. Xu, Y. Fang, M. Zhou, L. Liang, S. Singh, H. Zhao, A. Schober, Y. Lei, *J. Am. Chem. Soc.* **2015**, *137*, 3124 – 3130; c) Y. Liang, Z. Chen, Y. Jing, Y. Rong, A. Facchetti, Y. Yao, *J. Am. Chem. Soc.* **2015**, *137*, 4956 – 4959.

[7] S. Nishida, Y. Yamamoto, T. Takui, Y. Morita, *ChemSusChem* **2013**, *6*, 794 – 797.

[8] a) R. Raccichini, A. Varzi, S. Passerini, B. Scrosati, *Nat. Mater.* **2015**, *14*, 271 – 279; b) Z. Song, T. Xu, M. L. Gordin, Y. B. Jiang, I. T. Bae, Q. Xiao, H. Zhan, J. Liu, D. Wang, *Nano Lett.* **2012**, *12*, 2205 – 2211; c) T. Nokami, T. Matsuo, Y. Inatomi, N. Hojo, T. Tsukagoshi, H. Yoshizawa, A. Shimizu, H. Kuramoto, K. Komae, H. Tsuyama, J. Yoshida, *J. Am. Chem. Soc.* **2012**, *134*, 19694 – 19700; d) Z. Zhu, J. Chen, *J. Electrochem. Soc.* **2015**, *162*, A2393 – A2405; e) K. Zhang, Z. Hu, Z. Tao, J. Chen, *Sci. China Mater.* **2014**, *57*, 42 – 58.

[9] J. Song, M. Zhou, R. Yi, T. Xu, M. L. Gordin, D. Tang, Z. Yu, M. Regula, D. Wang, *Adv. Funct. Mater.* **2014**, *24*, 5904 – 5910.

[10] a) L. Z. Fan, Y. S. Hu, J. Maier, P. Adelhelm, B. Smarsly, M. Antonietti, *Adv. Funct. Mater.* **2007**, *17*, 3083 – 3087; b) Y. Shi, L. Peng, Y. Ding, Y. Zhao, G. Yu, *Chem. Soc. Rev.* **2015**, *44*, 6684 – 6696; c) Y. X. Yin, S. Xin, Y. G. Guo, L. J. Wan, *Angew. Chem. Int. Ed.* **2013**, *52*, 13186 – 13200; *Angew. Chem.* **2013**, *125*, 13426 – 13441; d) S. Srivastava, J. L. Schaefer, Z. Yang, Z. Tu, L. A. Archer, *Adv. Mater.* **2014**, *26*, 201 – 234; e) W. Li, Q. Zhang, G. Zheng, Z. W. Seh, H. Yao, Y. Cui, *Nano Lett.* **2013**, *13*, 5534 – 5540.

[11] a) D. Shao, H. Zhong, L. Zhang, *ChemElectroChem* **2014**, *1*, 1679 – 1687; b) P. R. Das, L. Komsiyska, O. Osters, *J. Electrochem. Soc.* **2015**, *162*, A674 – A678; c) J. M. Kim, H. S. Park, J. H. Park, T. H. Kim, H. K. Song, S. Y. Lee, *ACS Appl. Mater. Interfaces* **2014**, *6*, 12789 – 12797; d) D. H. Yoon, S. H. Yoon, K. S. Ryu, Y. J. Park, *Sci. Rep.* **2016**, *6*, 19962.

[12] A. Elschner, S. Kirchmeyer, W. Lovenich, U. Merker, K. Reuter, PEDOT: Principles and Applications of an Intrinsically Conductive Polymer, CRC, Boca Raton, **2010**.

[13] A. R. Katritzky, W. Q. Fan, *J. Heterocycl. Chem.* **1988**, *25*, 901 – 906.

[14] K. Zhang, C. Guo, Q. Zhao, Z. Niu, J. Chen, *Adv. Sci.* **2015**, *2*, 1500018.

[15] a) Z. Song, H. Zhou, *Energy Environ. Sci.* **2013**, *6*, 2280; b) X. Han, G. Qing, J. Sun, T. Sun, *Angew. Chem. Int. Ed.* **2012**, *51*, 5147 – 5151; *Angew. Chem.* **2012**, *124*, 5237 – 5241; c) L. Li, R. Jacobs, P. Gao, L. Gan, F. Wang, D. Morgan, S. Jin, *J. Am. Chem. Soc.* **2016**, *138*, 2838 – 2848.

[16] a) H. Kim, D. H. Seo, G. Yoon, W. A. Goddard III, Y. S. Lee, W.-S. Yoon, K. Kang, *J. Phys. Chem. Lett.* **2014**, *5*, 3086 – 3092; b) W. Walker, S. Grugeon, O. Mentre, S. Laruelle, J. M. Tarascon, F. Wudl, *J. Am. Chem. Soc.* **2010**, *132*, 6517 – 6523; c) W. Luo, M. Allen, V. Raju, X. Ji, *Adv. Energy Mater.* **2014**, *4*, 1400554.

[17] a) M. Park, D. S. Shin, J. Ryu, M. Choi, N. Park, S. Y. Hong, J. Cho, *Adv. Mater.* **2015**, *27*, 5141 – 5146; b) Z. Song, H. Zhan, Y. Zhou, *Angew. Chem. Int. Ed.* **2010**, *49*, 8444 – 8448; *Angew. Chem.* **2010**, *122*, 8622 – 8626.

[18] M. Lee, J. Hong, H. Kim, H. D. Lim, S. B. Cho, K. Kang, C. B. Park, *Adv. Mater.* **2014**, *26*, 2558 – 2565.

[19] S. Garreau, G. Louarn, J. P. Buisson, G. Froyer, S. Lefrant, *Macromolecules* **1999**, *32*, 6807 – 6812.

[20] G. García, M. Atilhan, S. Aparicio, *Phys. Chem. Chem. Phys.* **2016**, *18*, 4760 – 4771.

[21] J. B. Metson, S. J. Hay, H. J. Trodahl, B. Ruck, Y. Hu, *Curr. Appl. Phys.* **2004**, *4*, 233 – 236.

Received: January 31, 2016
Revised: March 8, 2016
Published online: April 15, 2016

  